COARSE-GRAINED MODELING OF INTERACTIONS OF NANOPARTICLES WITH LIPID MEMBRANES

By

PARVA KISHORKUMAR PATEL

A thesis submitted to the

School of Graduate Studies

Rutgers, The State University of New Jersey

In partial fulfilment of the requirements

For the degree of

Master of Science

Graduate Program in Chemical and Biochemical Engineering

Written under the direction of

Alexander V. Neimark

And approved by

_____

_____

_____

New Brunswick, New Jersey

May, 2019

ABSTRACT OF THE THESIS

COARSE-GRAINED MODELING OF INTERACTIONS OF NANOPARTICLES WITH LIPID MEMBRANES

By PARVA KISHORKUMAR PATEL

Thesis Director:

Alexander V. Neimark

Research of the mechanisms of interactions between nanoparticles (NPs) and lipid bilayers (LBs), which constitute the foundation of cell membranes, is important in order to understand not only the specifics of NP drug delivery and imaging but also to understand the harmful effects related to NP toxicity. In this work, a coarse-grained molecular dynamics (CGMD) with implicit solvent is used to elucidate the stability of LBs supported on silica substrates decorated with hydrophilic and hydrophobic NPs. We reproduce the experimental observation that large NP (>22 nm) can be coated by stable LBs, while smaller NPs (<22 nm) induces holes in the membrane. This result was achieved due to introducing novel features in CGMD set-up, which (a) secure the isotention membrane condition and (b) account for long-range lipid-substrate interactions due to the existence of the nanometer thick hydration layers between LB and silica. The latter effect is incorporated by using the effective long-range potential of interactions between lipid heads and silica mimicking the disjoining pressure developed in the hydration layer. The proposed GCMD method allowed for simulation of large systems with up to 40 nm NPs in the simulation cell of $231 * 154 * 77\ nm^3$ in volume. The method can be extended and applied to other NP-membrane systems, specifically to study the membrane stability affected by the presence of host bodies.

ACKNOWLEDGEMENTS:

I am deeply thankful to my advisor Professor Alexander V. Neimark and the group members, Dr Aleksey Vishnyakov, Dr Kolattukudy P. Santo, and Sean Burgess for their immense support, guidance and suggestions during the course of this work. This collaborative work is supported in parts by the NSF CBET Award "Adhesion and Translocation of Nanoparticles through Lipid Membranes", grant No.1510993 and Rutgers Bush Biomedical Bridging Grant Program.

TABLE OF CONTENTS:

1. Introduction:

1.1 Background and Motivation:

Lipid bilayers (LB) constitute the foundation of cell membranes and serve as barriers and the interface between the cell and its environment. In order to develop new biomedical nanotechnologies like bio-imaging and drug delivery, for lipid-mediated synthesis of NP, or biosensing with NP-doped supported lipid bilayers (SLB), it is necessary to understand the effects of LB interactions with host particles like nanoparticles (NP), proteins, receptors, membrane/tissue fragments, and other bio-ingredients.[1-3] When NP comes in contact with the LB, it may either adhere to the membrane outer surface or penetrate inside. The latter process may lead to the pore formation in the LB that can be useful in biomedical applications, like drug delivery, and harmful in case of inhaled and digested NP.

In recent years, SLBs have generated research interest due to their applications in many areas.[4-8] They can be used as a simplified model system in studies aimed at improving the understanding of the properties and functions of biological membranes or for experimental characterization techniques like NMR or FTIR[10], for lateral diffusion measurements[11] or for biosensing with NP-doped supported lipid bilayers (SLB)[3]. An important phenomenon associated with SLBs is the presence of the hydration layer formed by water molecules between substrate and LB. Many experimental studies[12-22] and simulation studies[9, 23-27] were conducted to understand this phenomenon. It was found that

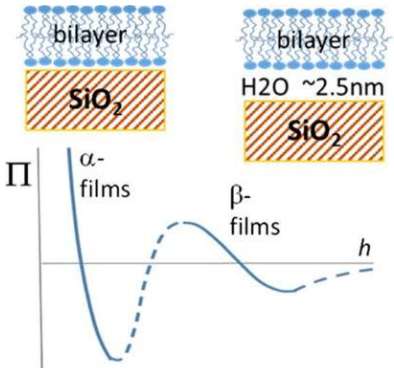

Figure 1.1.1: Disjoining pressure of double sigmoidal shape with two minima and one maximum, which correspond to the limits of stability of α-states and β-states.[9]

due to the existence of the hydration layer, the LB upon approach to the substrate feels the repulsive force, whereas there is a strong adhesion force preventing its detachment. This effect was quantified by the disjoining pressure. Vishnyakov et. al.[9] with the help of atomistic molecular dynamics calculated the disjoining pressure isotherm $\Pi(h)$ as a function of the separation between LB and hydroxylated amorphous silica; h represents the effective thickness of the hydration layer. This isotherm has a double sigmoidal shape with two minima and one maximum which corresponds to the limits of stability of the equilibrium states, called the α and β-states figure 1.1.1.[9] In α-state, the LB is in close contact with surface hydroxyls; however, because of the molecular level roughness of the amorphous silica surface, there exists an inhomogeneous distribution of water molecules trapped between the substrate and the LB. In β-state, the membrane is separated from the silica surface by the hydration film of ~2.5 nm in thickness that is stabilized by the specific interactions characteristic to thin water layers.

In many cases, NP adhesion to cell membranes is affected by physico-chemical factors such as particle size and shape, hydrophobicity, charge density, and physisorption of lipids and proteins rather than by specific biochemical interactions. In experimental atomic force microscopy studies Roiter et al. [28, 29] have discovered a critical size

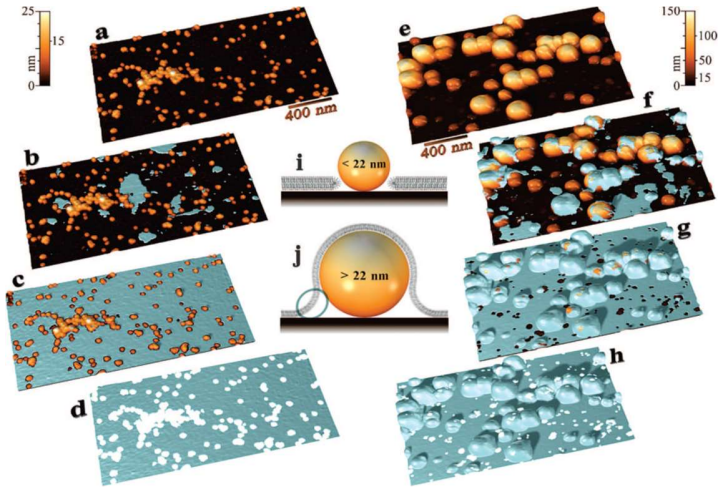

Figure 1.1.2[28-29] Lipid bilayer formation in the presence of particles larger than lipid bilayer thickness. AFM images (left) of lipid bilayer formation over a surface with 5–20 nm silica nanoparticles (a-d): (a) substrate with particles and no lipid, (b) surface partially covered by lipid bilayer (shown in silver color), (c) lipid bilayer formed on the substrate, (d) image of the lipid bilayer after "subtraction" of the particles and the substrate. AFM images (right) of lipid bilayer formation over the surface with mixed 5–140 nm silica particles (e-h): (e) the substrate with particles and no lipid, (f) partial coverage of the surface by lipid bilayer, (g) lipid bilayer formed on the substrate, and (h) image of the lipid bilayer after "subtraction" of the particles and the substrate. Schematics in the center illustrate how the lipid bilayer forms a pore around particles smaller than 22 nm (i) and how it may envelope the larger particles (j). The structure of bilayer area encircled in (j) is speculative because it cannot be resolved or assumed from AFM experiments.

dependence of the silica NP coating by supported dimyristoyl phosphatidylcholine (DMPC) lipid membrane: only particles larger than 22 nm or smaller than 1.2nm were blanketed by the membrane, while particle from 1.2 to 22 nm remained uncoated and formed nanoholes in the membrane (figure 1.1.2). Another observation was made by Lu et al, who measured the rates of silica NPs trans-membrane penetration into HeLa cells and found a non-monotonic dependence on the particle size with a maximum at ~50 nm.[30] Lin and Haynes[31] found a sizable difference between nonporous and porous silica particle leading to the damage of red blood cells. Burgess et. al.[32] performed dissipative particle dynamics (DPD) simulations to study the NP-induced rupture of LBs under tension. They found that larger NPs destabilize the LB and rupture is initiated by the pore formation near the NP surface.[32]

In order to study the NP-SLB interactions, a coarse-grained (CG) approach is needed as atomistic simulation are computationally prohibitively expensive. For example, Vishnyakov et. al. were just able to model a LB with 92 lipids in the simulation box size of $5.21 \times 5.276 \times 19.08\ nm^3$, with the accessible time scale of 100ns.[9] To simulate the larger systems that are necessary to observe the interaction of NPs with SLBs within larger scales, we employ implicit solvent (IS) CGMD method. In this method, solvent molecules are removed and an external force is introduced to compensate the solvent interactions. These interactions are incorporated using density-dependent potentials,[33, 34] angular dependent potentials,[35] Lennard-Jones tuned potentials[36] or modified Lennard-Jones potentials[37] between the lipid beads. In this work, we use the model proposed by Cooke et. al.[37] that was found to reproduce the properties of the DMPC membranes.

1.2 Goals of this work:

The main goals of this work are to understand the mechanism of interaction of LBs decorated with hydrophilic surfaces and hydrophilic and hydrophobic NPs. We develop an original methodology based on an implicit solvent method that takes into account the effects of disjoining pressure between LB and hydrophilic surfaces. We model the disjoining pressure interaction using a long-range potential that reproduces disjoining pressure isotherm obtained from the atomistic simulations. Using these tools, we perform simulations for LB interactions with surfaces containing hydrophilic and hydrophobic NPs of various sizes and analyze how the NP-LB-substrate interactions affect the SLB morphological changes such as pore formations and NP coating. We compare the simulation results to the experimental work done by Roiter et. al.[28, 29]

2. Models and Methods:

2.1 Implicit Lipid Bilayer Model: We consider a system of a lipid bilayer membrane consisting 1,2-dimyristoyl-sn-glycero-3-phosphocholine (DMPC) supported by hydrophilic silica substrate with nanoparticles on the surface. The lipids are represented by

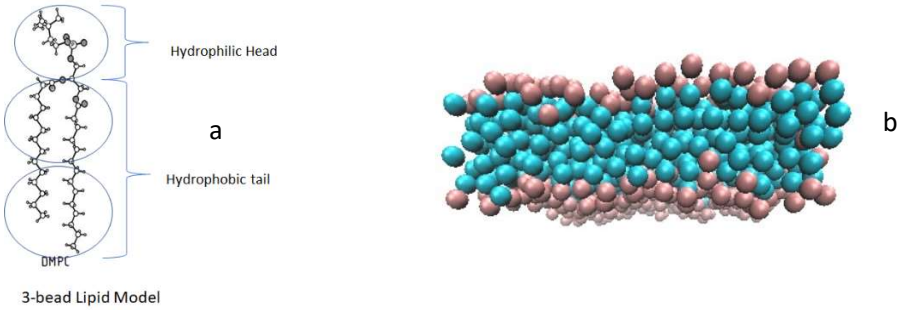

Figure 2.1.1: a) Coarse graining for DMPC molecule into 3 beads. b) Bilayer formed using Cooke-Desearno model[37]

an IS-CGMD model developed by Cooke and Desearno.[37] In this model, the lipid molecule is represented by three coarse-grained beads, one head bead and two tail beads as seen in fig. 2.1.1.a. The solvent effects are implemented by choosing the interaction potentials between the beads as a combination of a hardcore repulsive and a long-range attractive interaction. All beads interact with the repulsive Weeks-Chandler-Andersen potential,

$$V_{rep}(r;b) = \begin{pmatrix} 4\epsilon\left[\left(\frac{b}{r}\right)^{12} - \left(\frac{b}{r}\right)^{6} + \frac{1}{4}\right], r \le r_c \\ 0, r > r_c \end{pmatrix} \quad (1)$$

where ϵ and b is a unit of energy and effective size of the beads respectively. The cut-off for repulsive interactions is set to $r_c = 2^{\frac{1}{6}}b$. The tail beads interact with the effective long-range attractive potential:

$$V_{cos}(r) = \begin{cases} -\epsilon, & r < r_c \\ -\epsilon\cos^2\left[\frac{\pi(r-r_c)}{2w_c}\right], & r_c \le r \le r_c + w_c \\ 0, & r > r_c + w_c \end{cases} \quad (2)$$

Here, w_c is the tuning parameter which determines the range of the attraction. The sizes of the beads are taken to be $b_{hea\ ,hea} = b_{head,tail} = 0.95\sigma$ and $b_{tail,tai} = \sigma$, where σ is unit of length. The value of w_c is taken to be 1.5σ. Here, σ is equivalent to about 0.77nm. The attraction introduces the hydrophobic effect on tail beads and is necessary to obtain a LB self-assembly.

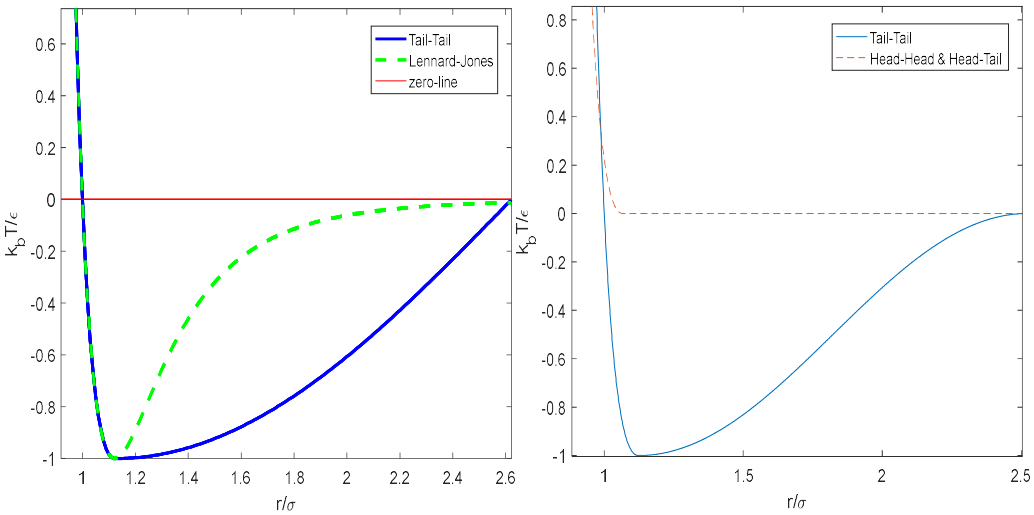

Figure 2.1.2: a) Comparison of Tail-potential with the Lennard Jones Potential. It shows slow decomposition of attractive force compared to LJ. b) Potential and distance relation for Head-Head and Tail-Tail

The head-tail (H-T) and tail-tail (T-T) bonds are modelled by the finite extensible nonlinear elastic (FENE) potential:

$$V_{bond}(r) = -\frac{1}{2}k_{bond}r_{\infty}^2 \log\left[1 - \left(\frac{r}{r_{\infty}}\right)^2\right], \quad (3)$$

with the stiffness $k_{bond} = 30\epsilon/\sigma^2$ and divergence length $r_\infty = 1.5\sigma$. In order to keep the lipids straight, the harmonic spring potential is used with rest length 4σ between the head bead and second tail bead,

$$V_{bend}(r) = \frac{1}{2}k_{bend}(r - 4\sigma)^2, \quad (4)$$

which corresponds in lowest order to a harmonic bending potential $\frac{1}{2}k_{bend}\sigma^2\vartheta^2$ for the angle $\pi - \vartheta$ between the three beads. The bending stiffness is fixed at $k_{bend} = 10\epsilon/\sigma^2$. Figure 2.1.2.a shows the interaction potential between tail-tail beads and how it is compared to Lennard-Jones potential. Figure 2.1.2.b shows the interaction potential between head-head, head-tail and tail-tail.

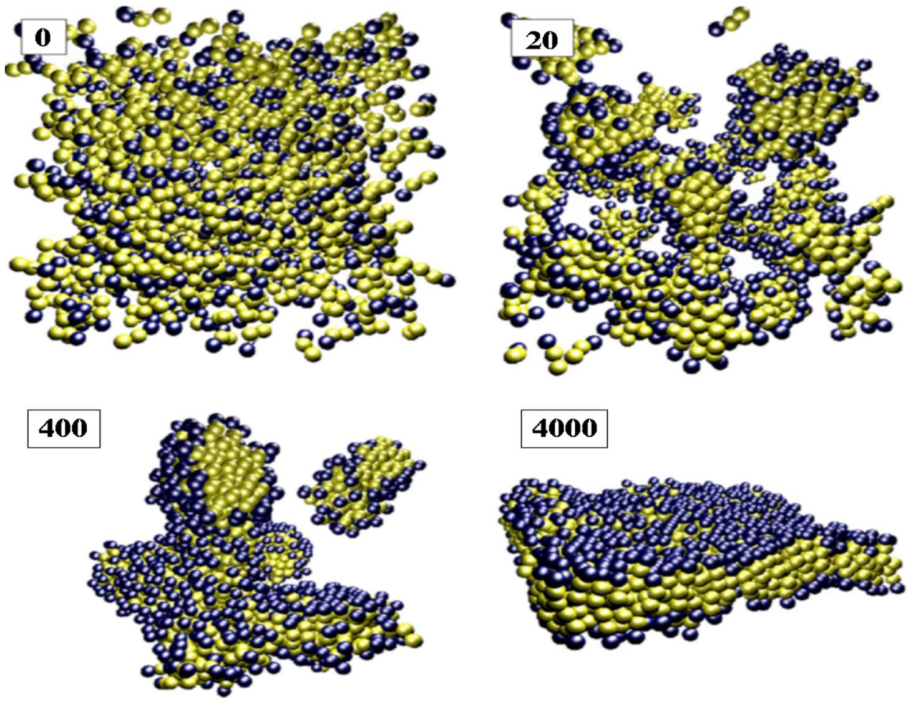

Figure 2.1.3[37]: Self-assembly sequence for the bilayer system with 1000 lipids in a cubic box of side length 25%. Lipid cohesion was set to $\frac{w_c}{\sigma} = 1.4(V_{Cos})$ and temperature to KbT=ϵ. Lipids quickly forms small clusters which slowly coarsen and eventually "zip up" to form a box-spanning bilayer sheet. The numbers indicate the simulation time and one-time step is equal to 10ns.

Fig 2.1.3 shows the evolution of LB self-assembly in the Cooke et. al.[37] model. Fig 2.1.4 a) shows the number density and its relation with the distance from the bilayer midplane. In Fig 2.1.4b) we can see the relation of the tension and the area of the bilayer. It can be

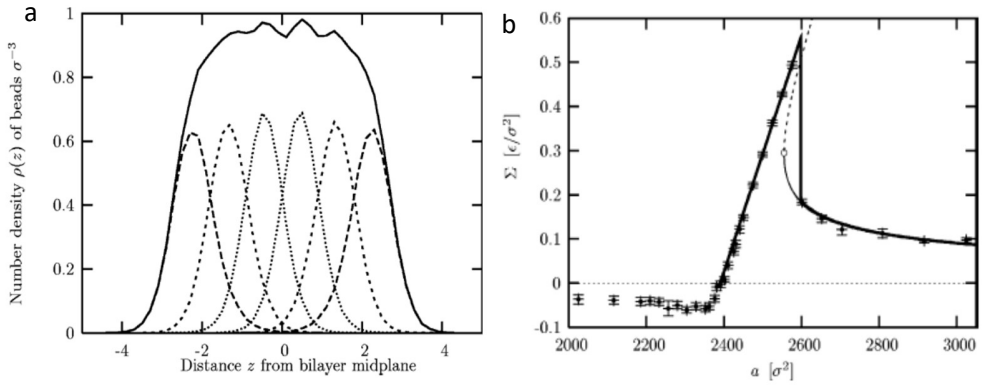

Figure 2.1.4[37]: a) Profile of the density as a function of vertical distance z from the bilayer midplane for a system of 4000 lipids at constant zero tension and with simulation parameters kBT=1.1ϵ and wc=1.6σ. The plotted lines are bead densities for head beads (long dashed), first tail beads (short dashed), terminal tail beads (dotted), and the sum of all beads (solid). b) Bilayer tension 5 as a function of (projected) area A for a flat membrane sheet with wc /σ =1.6 at kBT/ϵ =1.1. The bold solid line is a fit to the model of Farago[36] and Tolpekina *et al.*[39]

seen that as the LB is stretched the LB tension increases. After $0.55\epsilon/\sigma^2$ the LB undergoes a sudden decrease in the tension because of the pore formation in the LB. Upon further stretching, the pore size grows but the tension remains relatively constant.

2.2 Substrate Model: To model hydrophilic substrate surfaces we use a single layer of beads arranged in a hexagonal close packing (hcp) lattice, forming a homogeneous flat surface. The substrate beads interact with lipid beads through Weeks-Chandler-Andersen potential and an additional long-range potential is implemented between the substrate and LB heads in order to reintroduce the effect of disjoining pressure in this implicit solvent model as discussed in the next chapter. For the system consisting of 1800 lipids, the substrate has 2275 beads with dimension $42.35 \times 0.77 \times 26.95\ nm^3$ in X, Y and Z respectively; in the 4800 lipids system has 5970 beads and dimension $69.69 \times 0.77 \times 41.97\ nm^3$ in X, Y and Z respectively; in the 20000 lipids system has 19000 beads and

dimension $126.28 \times 0.77 \times 77.00\, nm^3$ in X, Y and Z respectively and in the largest 80000 lipids system, the substrate has 84000 beads and dimensions $270.00 \times 0.77 \times 154.00\, nm^3$ in X, Y and Z respectively.

2.3 Derivation of Head-Substrate Potential mimicking the Disjoining Pressure: With an implicit solvent model, a special long-range potential has to be introduced to account for the disjoining pressure effects. The potential is applied between the lipid head beads and substrate beads. Similarly, the same potential is applied between the head beads and the nanoparticle surface beads. It is assumed that the disjoining interactions are only between the single layer of substrate beads and the inner layer of head beads that is closer to the substrate. We also assume that both LB and the substrate are flat.

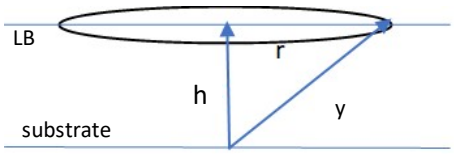

Figure 2.3.1: representation of flat layers of substrate and LB heads

The disjoining pressure can be expressed as,

$$\Pi_D = -\frac{1}{A}\left(\frac{\partial E_{SB}}{\partial h}\right)_{T,V,A} \tag{5}$$

where E_{SB} is the free energy of the membrane-substrate interaction, A is the surface area of the LB and h is the normal distance between the substrate and the membrane surface. As shown in the figure 2.3.1, the head beads of the membrane placed at a distance h interact with the substrate bead via pairwise distance y. The substrate bead feels the equal-interaction potential of the head group beads located at the circle of radius r, where $r = \sqrt{y^2 - h^2}$. If $V(y)$ is the pair-wise interaction potential between a membrane bead and a substrate bead, then the total interaction felt by the substrate bead by the membrane beads

at a distance y from the center of the bilayer surface ($r = 0$) is, $V_{SB}(y,h) = V(y)2\pi r\, dr\rho_B$, where ρ_B is the number of membrane beads per unit area of the surface.

Total interaction potential between the substrate bead and the LB is expressed as,

$$V_{SB}(h) = 2\pi\rho_B \int_0^\infty V(y)\, r\, dr \tag{6}$$

assuming that the membrane is homogeneous and ρ_B is constant. Changing variable from r to y, we have $dr = \frac{1}{\sqrt{y^2-h^2}}\, y\, dy$. That is, $r\, dr = y\, dy$ and the limits of integration is from h to ∞. Thus, we have

$$V_{SB}(h) = 2\pi\rho_B \int_h^\infty V(y)\ y\, dy \tag{7}$$

Since both substrate and membrane are assumed to be homogenous, the total membrane-substrate interaction energy at a separation h is given by adding contributions from all substrate beads,

$$E_{SB}(h) = N_S V_{SB}(h) = 2\pi N_S\, \rho_B \int_h^\infty V(y)\ y\, dy \tag{8}$$

where N_S is the total number of beads on the substrate surface. The disjoining pressure is related to the introduced head-substrate potential $V(y)$ as,

$$\Pi_D = -\frac{2\pi N_S \rho_B}{A}\frac{\partial}{\partial h}\left(\int_h^\infty V(y)\, y dy\right) \tag{9}$$

The interaction potential vanishes at long distance, and the disjoining pressure becomes

$$\Pi_D = \frac{2\pi N_S \rho_B}{A} V(h)h \tag{10}$$

Thus, we have

$$V(h) = \frac{\Pi_D}{2\pi\rho_S\rho_B\, h}, \qquad (11)$$

where $\rho_S = N_s/A$, the surface number density of substrate beads. V is then used as a pairwise interaction between bilayer heads and substrate.

Using Eq. 11 and disjoining pressure values from MD simulations of Vishnyakov et. al.[9] we develop a pairwise interaction potential $V(h)$ and force between substrate and lipid heads as shown in the figure 2.3.2. It must be noted Vishnyakov et. al, the water thickness was measured whereas we need center-to-center distance between lipid heads and substrate. So, considering $\sigma = 0.77$ nm and size of the bead as 1σ (radius 0.5σ), for the

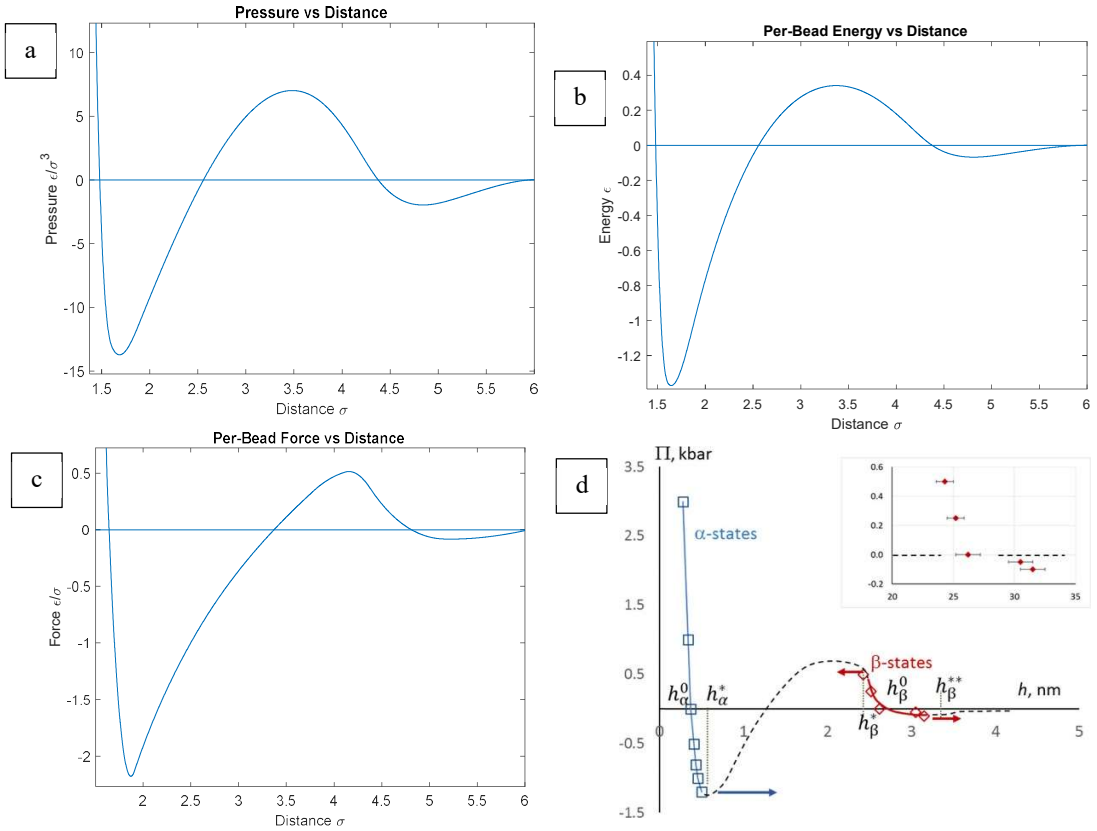

Figure 2.3.2 a) Spline plot derived from the disjoining pressure values from Vishnyakov et. al. **b)** head-substrate potential which replicates disjoining pressure **c)** Forces derived from the potential **d)** Disjoining pressure as observed by Vishnyakov et. al.[9]

water thickness of 0.37 nm (h_α^0), the pair distance between two beads is 1.48σ. The pressure data point from MD simulations are interpolated using the spline cubic fit, and the interpolated data is converted to the values of force and energy.

2.4 Nanoparticle Model: The NP is formed by the beads arranged into a 3D hcp lattice. The NP is designed to represent an approximately spherical particle carved out of a crystal, which maintains its fairly spherical shape as it is kept rigid. The inner layers of the NP are formed by core beads that strongly repel all other beads in the system (except the outer layer of the NP) to ensure that the NP is impenetrable. The shell layers of the NP consist of hydrophobic or hydrophilic beads depending on the system studied. NP parameters are provided in the following sections.

2.4.1 Particles smaller or equal to the thickness of bilayer: The smaller particles

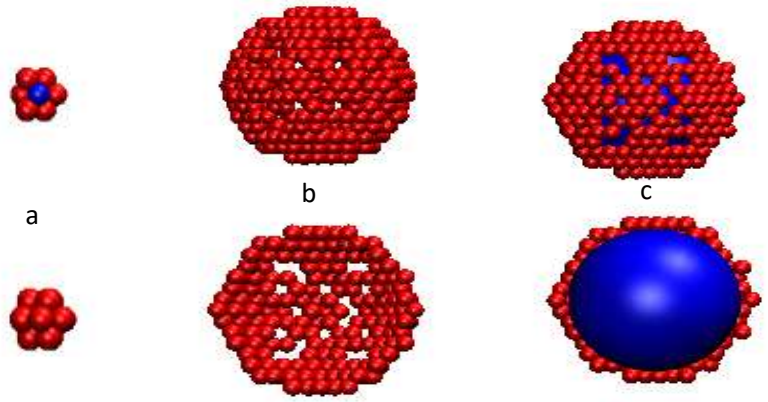

Figure 2.4.1: a) Shows how the small particles are made up of the cross section view shows the inner core which will prevent the lipids the enter the NP b) Hydrophilic particle with no core beads as due to disjoining pressure none of the beads are penetrating c) Large hydrophobic particle which is made up of only single large bead which will prevent the lipids from entering the NP.

considered here are NPs with diameter 1.54 nm, 3.08 nm, 4.62 nm. NP with diameter 1.54 nm consists of 13 beads in which 12 are shell beads and 1 bead consist of an inner core. The 3.08nm NP consist of 57 beads in which 38 beads are shell beads and 19 beads are

inner core beads. The 4.62 nm NP consists of 159 beads in which 72 are shell beads and 87 beads are inner core beads.

2.4.2 Larger particles: Large nanoparticles are composed of beads in HCP lattice with a single large core bead that acts like a hardcore shell so no beads can penetrate inside. The hardcore shell effect is modelled using Weeks-Chandler-Andersen potential with r_c =diameter of the NP. We are using NPs with diameter 9.24 nm, 15.4 nm, 23.1 nm and 40.04 nm to study the interactions for supported lipid bilayers. NP with diameter 9.24 nm consists of 402 shell beads, 15.4 nm consists of 1022 shell beads, 23.1 nm consists of 2396 shell beads and 40.04 nm consists of 6924 shell beads.

2.5 System Setup: In order to secure the isotension conditions, the bilayer is attached to the frame with two solid planks (see fig 2.5.1) using the tail-tail potential (Eq. 11) between bilayer tails and the center region of the planks (brown beads). The planks are made up of 2 layers of beads in hcp lattice. The top and bottom third of the inner layer and the 2nd layer of planks consist of purely repulsive beads towards all beads of the LB in order to prevent lipids from wrapping around the plank. The role of planks is to hold the bilayer and provide the constant tension conditions which can be achieved by restricting the movement of one of the planks and allowing one of the planks to move only in the lateral direction. Isotension condition is maintained at 0.2 ϵ/σ^2 corresponding to the lipid density of 1.6 beads/σ^2 in DMPC LB. The system is equilibrated far from the substrate so there is no interaction between LB and substrate/NP. The NP is placed just above the substrate and both NP and substrate are static throughout the equilibration.

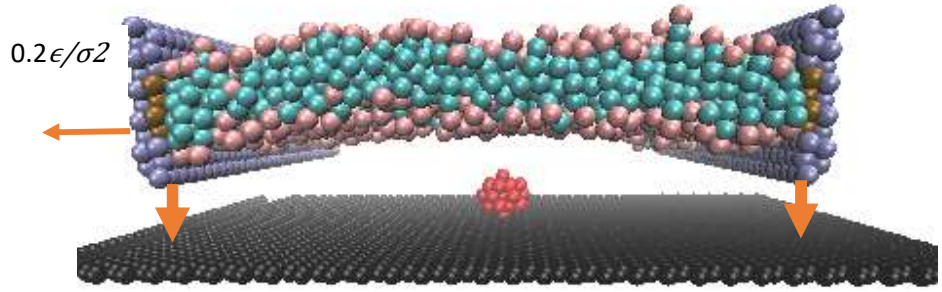

Figure 2.5.1: Simulation setup showing the isotensed LB between the frames and how the LB is moved onto the substrate.

2.6: Interaction of LB with Silica Substrate: In order to validate the long-range pair potential to reproduce the disjoining pressure effect, we simulate the PV - substrate system and move the bilayer towards the substrate by allowing the planks to move in the y-direction. A constant force is applied to all head beads closest to the substrate which causes the entire system to approach the substrate. Note, when we attempted to apply a constant force to all lipid beads, it caused the lipids to flip with tails towards the substrate and heads away. This happened because the pairwise disjoining pressure potential is only applied to head beads, which had the undesirable consequence of distorting the LB. We gradually increase the force on the bottom heads and calculate their mean position. From the force applied the position of LB position is obtained, the disjoining pressure is then calculated as a function of h.

2.7 β-state Simulations: In this case, we simulate systems with nanoparticles situated on the substrate, with LB initially placed far from the substrate without imposing the pairwise interaction between LB heads and the NP and substrate surface beads. Then the LB is moved to the β-state by applying a very small force on all LB beads of magnitude 0.001 $\frac{\epsilon}{\sigma}$ and by moving the planks with a velocity v_{plank} ($v_{plank} = 0.001\ \sigma/\tau$ for smaller particle and 0.0025-0.005 σ/τ for large particles). As the LB approaches the β-state, the

constant velocity condition is removed. After the LB position stabilizes, all the external applied forces are removed, the planks are allowed to freely move in the y-direction and the LB finds its equilibrium position in the β-state.

2.8 α -state Simulations: The bilayer in the α-state is simulated with a similar procedure, as section 2.7, except that to overcome disjoining pressure barrier, that is not easy for the bilayer to cross without some external force, we initially shorten the cut-off of the disjoining pressure to 2.55σ and then allow the bilayer to move to the α state. After it has reached the α-state, the full disjoining pressure potential is applied. In this way, the conformations of the LB in the α-state is explored. Note, the validation process for the substrate without the NP, see section 3.1 below, is carried out through a continuous increase in the force with no special treatment given at the point where the LB jumps from the β-state to the α-state.

3. Results:

3.1 Interaction of LB with Silica Substrate: Validation of Disjoining Pressure Potential:

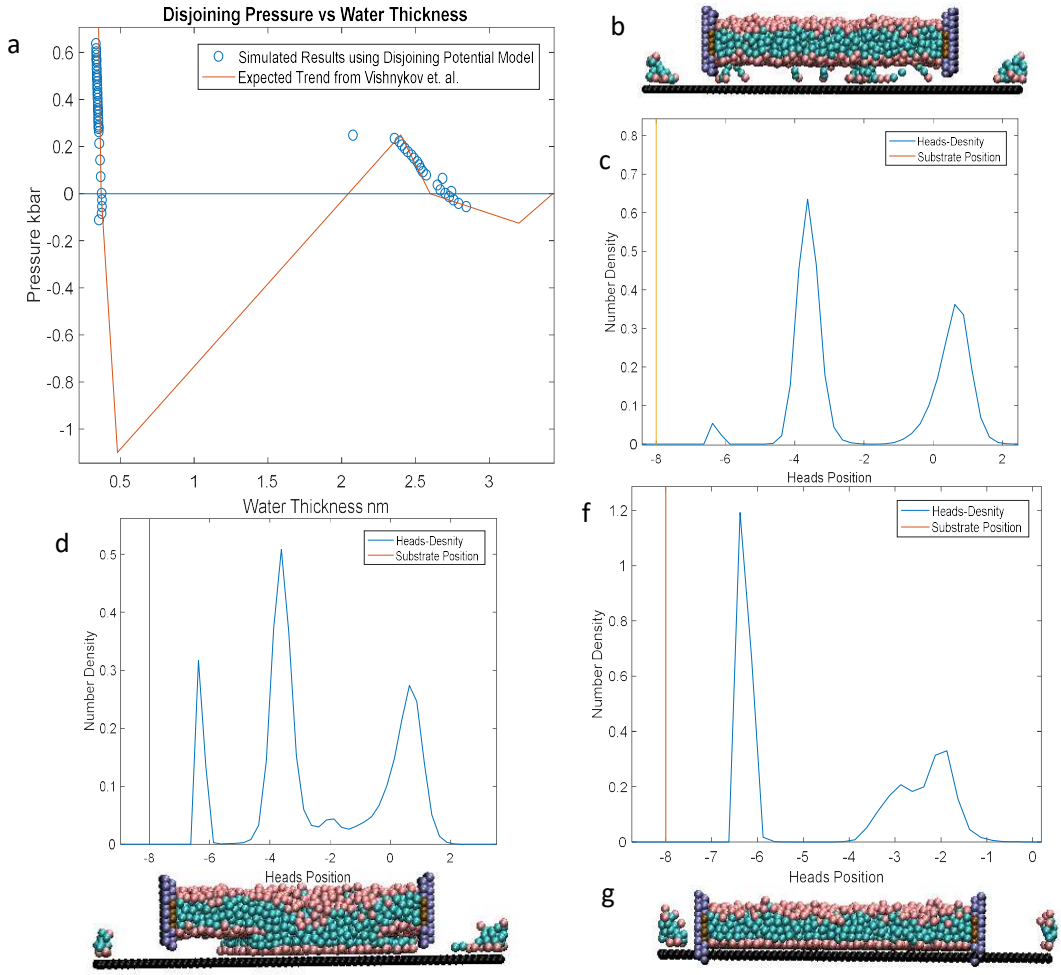

Figure 3.1.1: a) Shows the comparison between the simulation and the expected trend of the Vishnyakov et. al. b) heads density profile Critical point after which on increasing the force most of the bilayer will start going towards the substrate in α-state. b) Snapshot at critical point for pressure 2.6 kbar d) heads density when most of the beads moves towards the substrate overcoming the barrier in β-state. e) Snapshot which shows how the bilayer propagates from β-state to α-state for applied pressure of 2.7kbar. f) heads density when the bilayer has jumped to the $\alpha -$ state. g) Snapshot which shows the bilayer in the $\alpha -$state with close contact to substrate.

Figure 3.1.1 describes the results of the simulation for the validation of the disjoining potential. In this case, the interaction of the LB with the substrate that has no NP decorated on its surface is simulated. The force is applied on the LB beads to equilibrate LB at a mean

position above the substrate. The disjoining pressure corresponding to the applied force is plotted in Fig, 3.1.1 a, which shows very good agreement with the disjoining pressure from Vishnykov et. al.[4] Initially the LB is placed far from the beta state and then gradually pushed towards the substrate. The beta state at which the LB relaxes is found to be ~2.7 nm that is close to ~2.6 nm obtained in [4]. The snapshots and head group density profiles at various points as the bilayer is pushed from beta to alpha state are shown in Fig. 3.1.1 b-g. Generally, the density profiles of the bottom heads are narrower, because of the attraction from the substrate, while the top heads have a much broader distribution since they do not interact with the substrate and therefore do not feel any attraction. Increasing the force on the LB, we observe that a few lipids gain enough energy to cross the barrier, and the whole LB jumps toward the substrate after a certain critical force. This critical force is found to be equivalent to the pressure of ~0.26 kbar which is close to 0.25 kbar obtained by Vishnykov et al.[4] The □- state configuration of the LB is given in Fig. 3.1.1 f-g. Our model is able to reasonably reproduce the disjoining pressure in the regions of stability of the β-state from -0.08 kbar to 0.25 kbar and the α-state from 0.7 kbar to -0.1 kbar. Most interesting are the □- and □- states with zero disjoining pressure , which correspond to the equilibrum states that would be obtained in the process of unforced adhesion. Note, that the states with the negative values of the disjoining pressure correspond to experimental states that could be observed during the membrane detachment.

3.2 LB Coating of the Substrate with Hydrophilic Particle:

We performed simulations of systems consisting of the LB and the substrate with a hydrophilic NP of various sizes decorated on the surfaces. The LB configurations are analysed at both α-and β states by the procedures outlined in sections 2.7 and 2.8. In the β

state, we observe no effects on the LB, with very small NPs, while NP of intermediate sizes causes the formation of the hydrophilic pores. Larger NPs cause partial covering of the NPs by the LB. In the α-state, we observe, pore formation in the case of small NPs, while large NPs cause partial to complete coverage by the LB over the NP.

3.2.1 Hydrophilic NP with diameter 1.54nm: Figure 3.2.1 shows snapshots of the

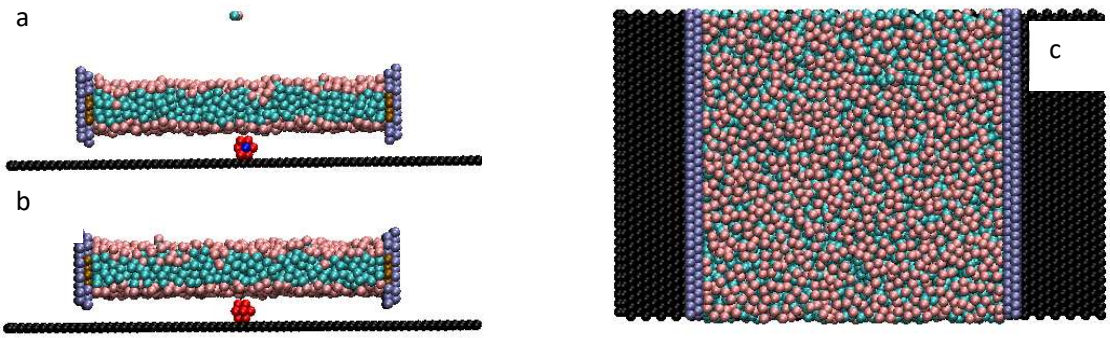

Figure 3.2.1: LB covering of substrate and 1.54nm Hydrophilic Particle: a) Final cross-sectional view, shows that there is no bulging but also shows that lipid is in α −state wrt NP b) Side view of the NP-LB interaction c) Top view where we don't see any pore formation.

simulations of LB in the β state, with the 1.54 nm NP on the substrate. The NP makes no influence on the LB in the β-state as can be seen from the cross-sectional (Fig. 3.2.1 c), side (Fig. 3.2.1 b) and top (Fig 3.2.1 a) views of the system. Although there is disjoining interaction between the LB and NP, it is so weak that no bulging or pore formation in the bilayer occurs. The LB is able to overcome barrier separating β and α-states.

The LB configuration in the α-state with 1.54nm NP is shown in Fig, 3.2.2. In this case, pore formation is observed, contrary to what is observed in the β state. The pore is slowly opened (Fig. 3.2.2 a) and is grown (Fig. 3.2.2 b) into a hole that is larger than the NP (Fig. 3.2.2 c). Also, the pore formed is a hydrophobic pore with no head groups at the rim (Fig. 3.2.2 c). This can be happening due to the disjoining pressure as the top head will have to cross the barrier which it is unable to do so. Also, looking at fig 3.2.2 b and fig

3.2.2 c it can be clearly understood that with respect to NP the heads beads favour staying in the β-state rather than the α-state due to the progression of the pore and this could be because of isotension nature of our LB.

While it is unlikely the pore would be hydrophobic in a real system, such a configuration is likely a deficiency of the model: the lipid molecules composed of just three beads are way too short and do not have sufficient flexibility to form a toroidal surface that is commonly observed on the edge of a pore in a lipid membrane. Additionally, there is very little to no energy penalty for a hydrophobic pore in this model.

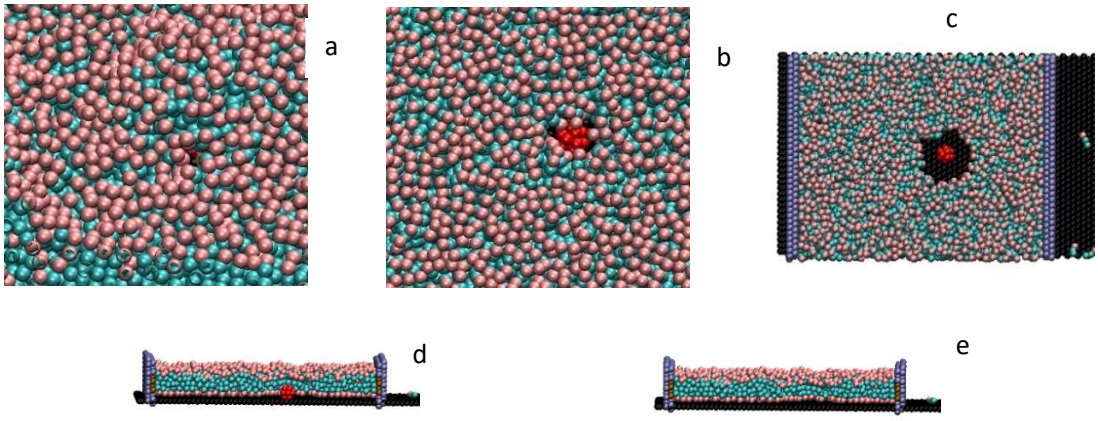

Figure 3.2.2: a) Shows the pore opening at 15.1 μs b) Flat pore after which propagation starts c) Final stable pore d) Cross Section View with NP shows the presence of cylindrical pore e) Shows hydrophobic pore.

3.2.2 Hydrophilic NP with diameter 3.08 nm and 4.62 nm: Figs. 3.2.3 & 3.2.5 illustrates

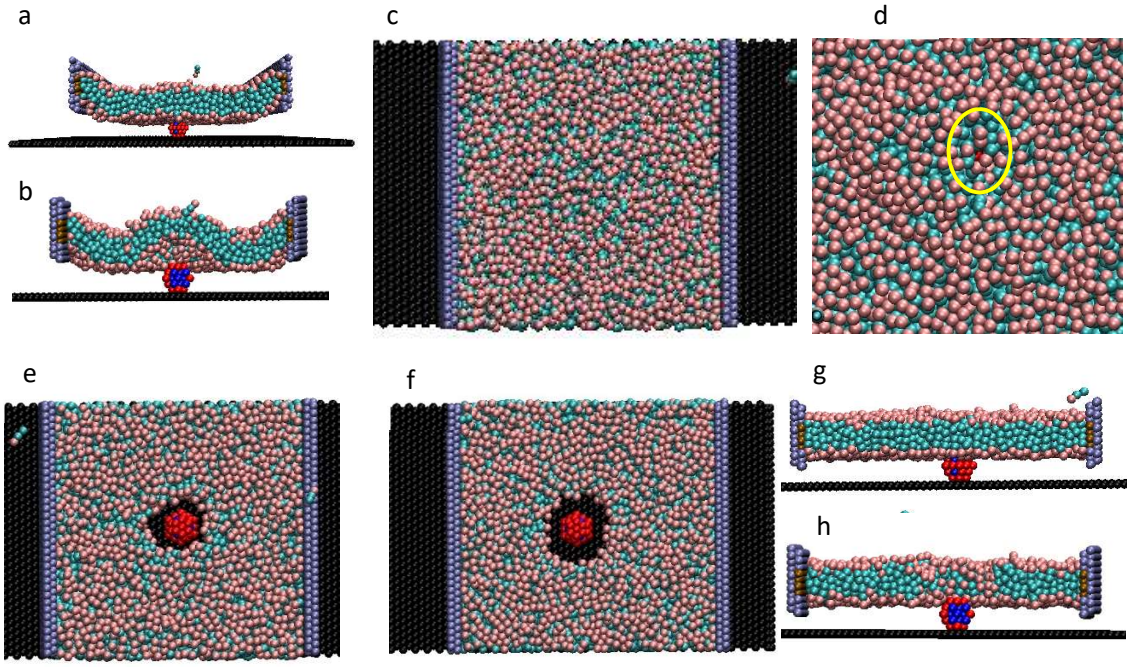

Figure 3.2.3: 3.08nm NP-LB Interaction a) shows the initial covering of the NP by LB when LB is still moving towards the substrate b) Shows clearly the bulging of the LB c) Show that bulging from the top d) Pore starting to form highlighted in yellow circle. Tiny red dot seen in NP e) Complete flat pre formation f) Final stable pore from the top g) Shoes how the bilayer with the pore has stabilized in the *β*-state h) Shows hydrophilic pore formation.

LB interaction with a substrate having NPs of diameter 3.08 nm and 4.62 nm on its surface, in the β-state configuration. From Fig. 3.2.3a we can see how the LB bends around the NP as it is brought towards the substrate from above. As the NP approaches the β state, a small pore opens which then expands (fig 3.2.3d and fig 3.2.5b) into a pore of diameter ~5.5 nm and ~7 nm in diameter respectively and stabilises (fig 3.2.3e and fig 3.2.5c). From

the cross-sectional view (fig 3.2.3d and fig 3.2.5e-f) it can be seen that the pore formed are

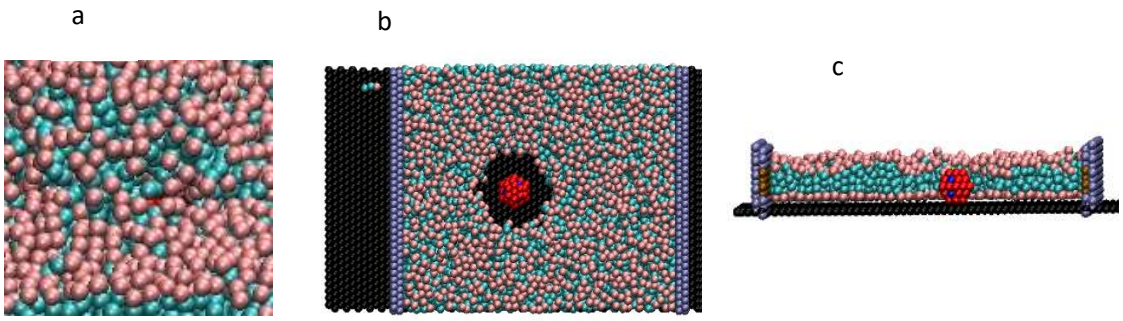

Figure 3.2.4: 3.08 NP-LB Interaction at α-configuration a) Small pore opening b) Propagation and formation of pores larger than NP diameter c) Hydrophobic pores.

hydrophilic in nature due to the presence of the head group near the rims.

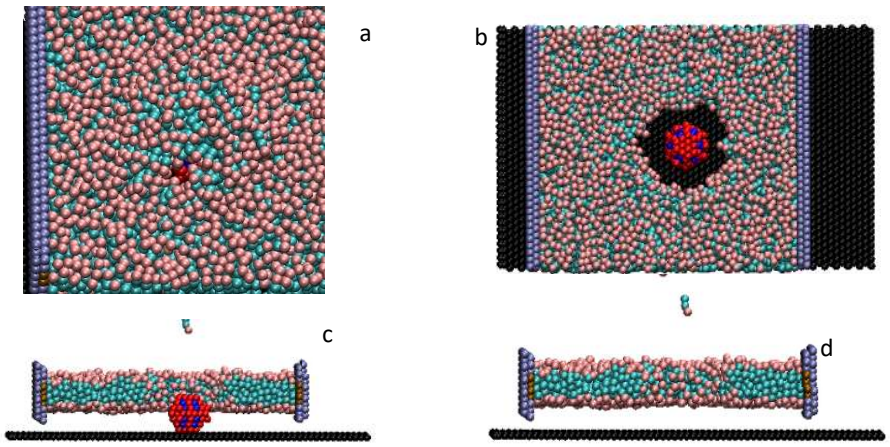

Figure 3.2.5: 4.62nm NP-LB interaction: a) shows in the pore opening b) shows the final stable pore c) Shows the hydrophilic pore formed d) Shows hydrophilic pore with NP.

Fig 3.2.4 and 3.2.6 shows the interaction at α-configuration. The dynamics of pore formation (fig 3.2.4a and fig 3.2.6a) and propagation to stable pore larger than NP diameter (fig 3.2.4b and fig 3.2.6b) is similar to what is stated for β-configuration but the only difference here is that the pore formed are hydrophobic in nature which is evident from cross sectional view (fig 3.2.4c and fig 3.2.6c), reason for such pores is discussed in 3.2.1.

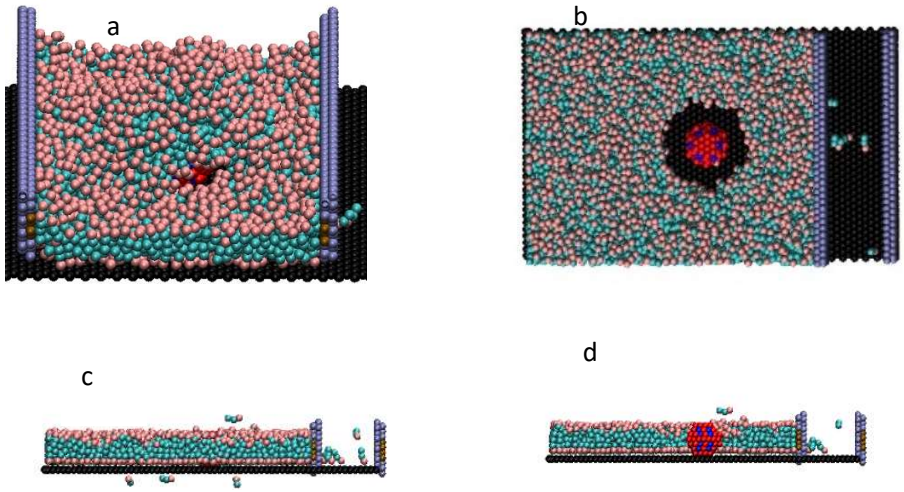

Figure 3.2.6: 4.62 nm NP-LB at α -state: a) Shows the pore opening b) Stable Final pore c) Shows side view of NP-substrate covering d) shows the formation of hydrophobic pore.

The pore formed for the 4.62 nm particle when bilayer is in the β- state is larger than the α-state as it is evident from the fig 3.2.6.b,c,d.

3.2.4 9.24nm and 15.4nm Nanoparticle:

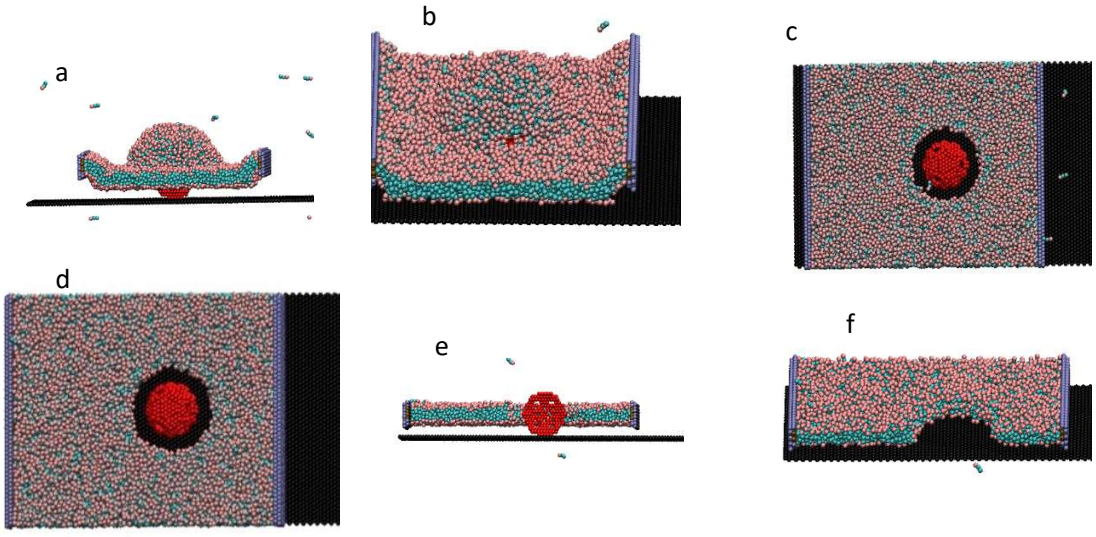

Figure 3.2.7: 9.24 nm β −state simulations: a) Shows the total covering of bilayer during propagation of bilayer towards the β −state b) Shows the small pore opening c) Shows the formation of the flat pore formation. d) shows the stable final pore. e) Cross-Sectional View where hollow nature of the NP is visible. Also, hydrophilic pore can be seen) Without NP hydrophilic pore is clearly seen.

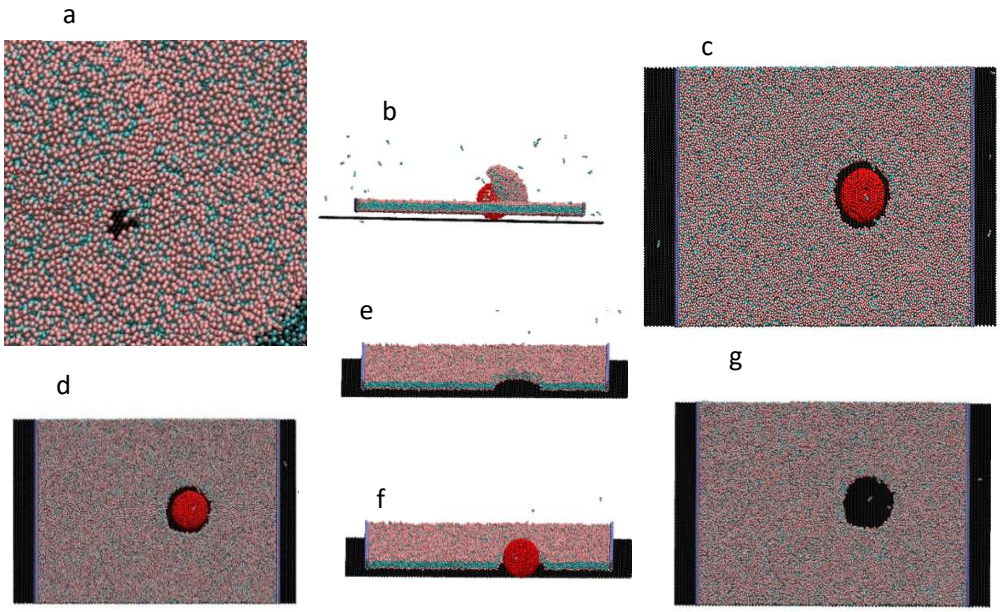

Figure 3.2.8: 15.4 nm NP-LB interaction in β- state a) Small pore opening b) semi covering of NP by bilayer c) Flat pore formation d) Stable final pore e) Shows the hydrophilic pore when NP is removed and f) shows the hydrophilic pore with NP g) top view of bilayer with pore without NP.

Fig 3.2.7 and Fig 3.2.8 shows the β-state configuration of LB above the substrate having the NPs of sizes 9.24 nm and 15.4 nm. As seen before, NP gets enveloped by the LB as it moves towards the substrate (Fig. 3.2.7a) and subsequently pores opening occurs (Fig. 3.2.7b and Fig 3.2.8a) which grow into a large pore. Here the pore diameter is ~12 nm and ~18nm for 9.24 nm and 15.4 nm NPs respectively due to head groups present near the rim of the pore that is in the β-state of the NP disjoining potential. This process of pore formation is so slow that if enough equilibration steps (approximately 250μs and 500μs for 9.24 nm and 15.4 nm NPs respectively) are not given then one might assume partial coating of that the bilayer (fig 3.2.8). The pore is hydrophilic which can be seen in (Fig 3.2.7e-f and Fig 3.2.8 e-f).

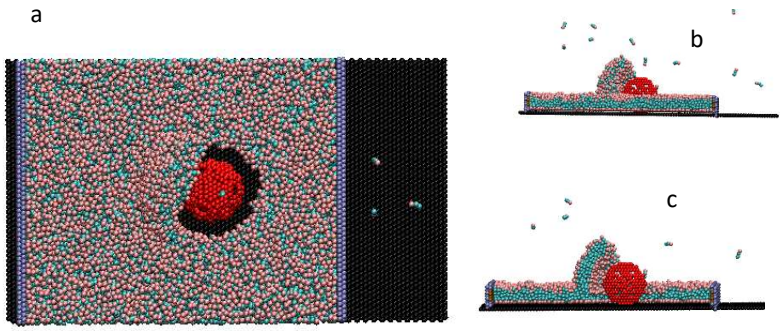

Figure 3.2.9: 9.24 nm NP-LB interaction in α-state: a) Top view we can see that there is partial coating of the LB b) Side view for partial coating c) Cross View which shows the hydrophobic pore

Figure 3.2.9 shows the 9.24 nm NP interaction with LB in α-state. From the figure, it is clear that there is a partial coating of LB on the NP and this coating is quite stable. We equilibrated LB for about 250μs and still, the coating was present.

3.2.5 23.1nm and 40.1nm Nanoparticle: In this case, we simulated a large system with

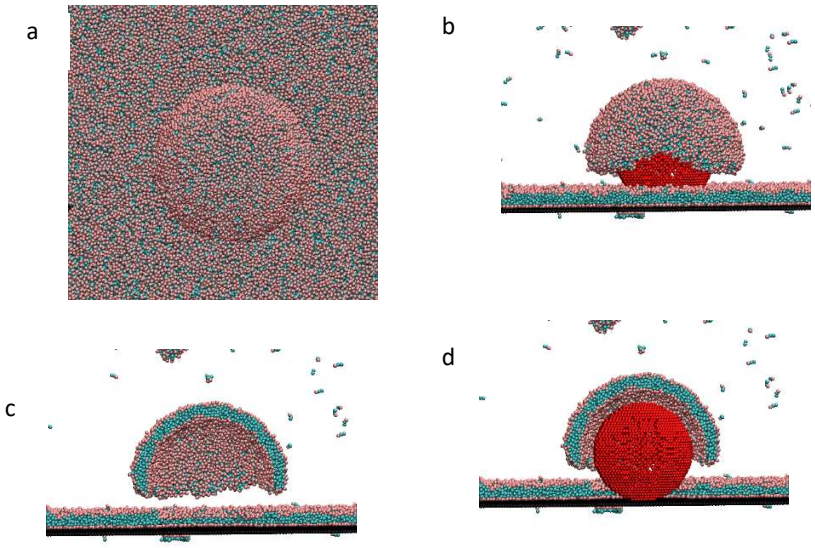

Fig 3.2.10 a) Top view shows the coating of NP b) Side view shows that the membrane has separated from the side c) Cross view without NP shows the hydrophobic pore d) Cross view with NP

bilayer containing 20000 lipids and 80000lipids, with a box size of $115 \times 77 * 77\ nm^3$ $231 \times 154 \times 77\ nm^3$ with 23.1 and 40.1 nm NP respectively on the substrate surface.

Figure 3.2.10 and figure 3.2.11 shows the snapshots of the final configuration of the LB in the α-state. The NP is mostly covered by the LB as seen by the top view (Fig 3.2.10a and 3.2.11a), however, the side views show Fig (3.2.10b-c-d and 3.2.11b-c) that the LB is broken at the NP-substrate contact and appear to be separated around the NP-substrate contact region.

3.3 LB Coating of the Substrate with Hydrophobic Particle:

In the case of substrates with hydrophobic NPs, we have analyzed only the LB configurations in the β-state. We study the effects of hydrophobic NPs of sizes 1.54nm, 3.08nm, 4.62nm, 9.24nm, 15.4nm and 23.1nm, that are placed on the hydrophilic substrate surface, on the LB that is brought towards the β-state from above. In general, the disjoining potential is absent between the NP-LB interactions, and as a result, the NP penetrates easily into the LB. For small NPs with a diameter smaller than the LB thickness, the NP is only partially encapsulated by the LB. As the NP size increases, the engulfing leads to monolayer coating on the NP. The results for NPs of different sizes are discussed in detail below.

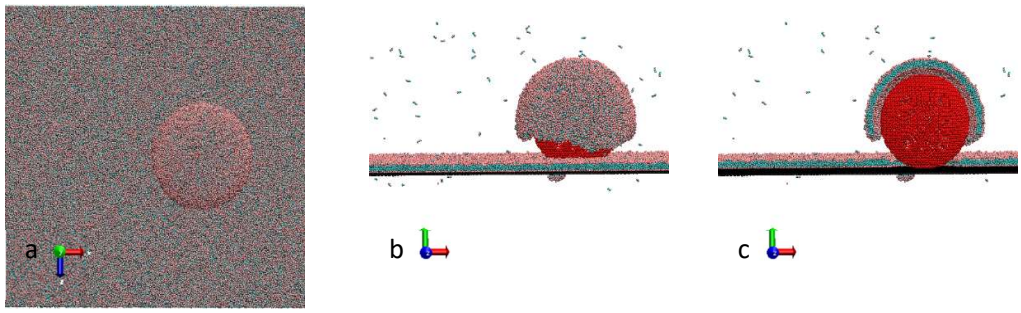

Figure 3.2.11: 40.1nm NP-Lb interaction at α-state: a) From top view NP coated by LB b) Side view where it can be seen that LB coated on NP is separated from LB on substrate c) Cross View shows the hydrophobic pore

3.3.1 1.54nm Nanoparticle: The interaction of small hydrophobic NP with diameter 1.54 nm resulted in no substantial changes in the LB configuration as there is no effective contact with the LB which is seen in the cross-sectional, side and top views (Fig.3.3.1).

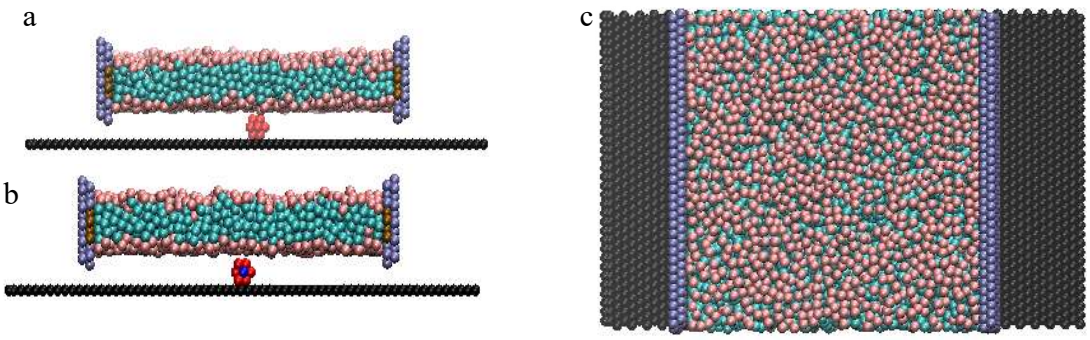

Figure 3.3.1: 1.54 nm hydrophobic NP-LB interaction: a) Side view where it can be seen how the bilayer rest on top of NP in β −state b) Cross-Section view which shows that there is no interaction between NP-LB c) Top view.

3.3.2 3.08 nm and 4.62 nm Nanoparticle: In this case**,** the NP is large enough to get in

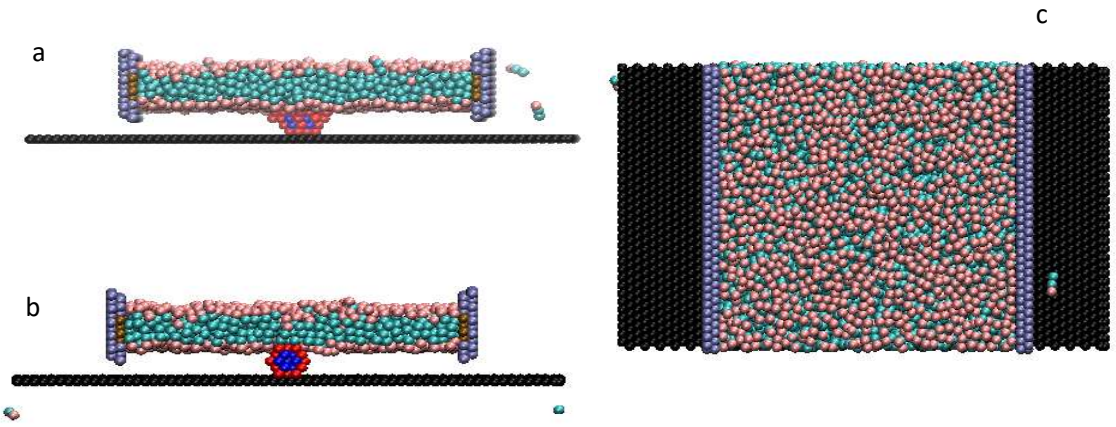

Figure 3.3.2: 3.08nm hydrophobic NP-LB Interaction: a) Side view shown the penetration of the NP-LB b) Cross View gives the better picture for the penetration c) Top View

contact with the LB which is stable in the β state. Being hydrophobic, the NP penetrates the bilayer as shown by the side and cross-sectional views (Fig. 3.3.2), however, the NP is not engulfed from the bottom side. This is mainly because when the LB engulfs the NP LB or monolayer bends or curves around the NP and some energy is spent during this process

and due to which it cannot overcome the β-state energy barrier and completely engulf the NP. Similar behaviour is observed for slightly larger NP with diameter 4.62 nm (see Fig.3.3.3).

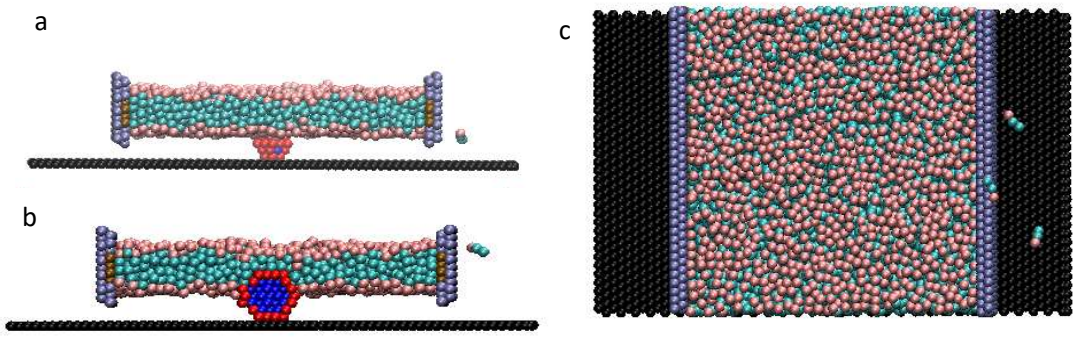

Figure 3.3.3: a) Clear penetration of NP into the bilayer b Cross View shows the penetration b) Top view

3.3.3 9.62 nm and 15.4 nm Nanoparticles: With larger NPs, we observe, engulfing of the NP by the LB with monolayer coating around the NP. In addition, we observe a tendency to cover the bottom part of the NP. This could be because, as the NP size become

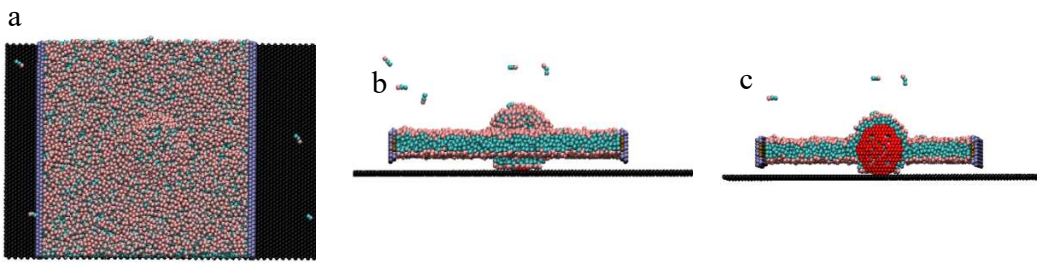

Figure 3.3.4: a) Shows the top View b) Shows the total encapsulation of the NP c) Shows the monolayer surrounding the NP.

larger the number of interactions increases and also as size increases the curvature of the bottom surface decreases, which allow the lipid tails to slide through, more easily, compared to the small NPs, in which the tails will have to move straight down to the substrate. Fig. a-c shows the LB configuration for 9.62 nm NP.

The dynamics for the 15.4 nm NP are similar to that of the 9.62 nm NP. Because of the

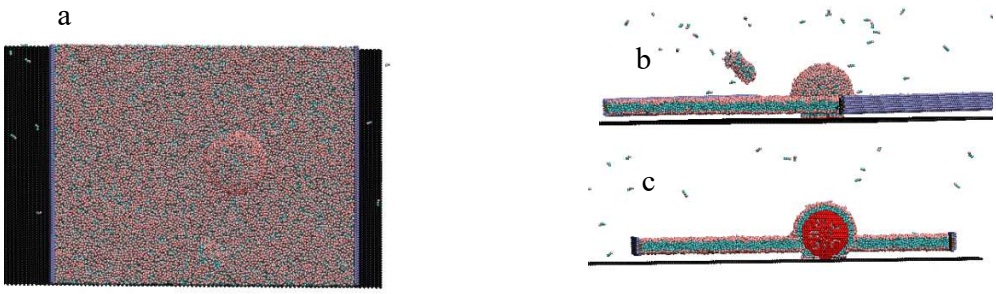

Figure 3.3.5: a) Shows the top View b) Shows the total encapsulation of the NP. There is a small micelle which was formed during the propagation of bilayer towards the substrate c) Shows the monolayer surrounding the NP.

size of the NP, LB envelopment requires significant disturbance of the LB structure. This disturbance causes many lipids to be thrown from the LB resulting in the micelle observed in figure 3.3.4b.

4. Conclusion:

Research of the mechanisms of interactions between nanoparticles (NPs) and lipid bilayers (LBs), which constitute the foundation of cell membranes, is important in order to understand not only the specifics of NP drug delivery and imaging but also to understand the harmful effects related to NP toxicity. In this work, a coarse-grained molecular dynamics (CGMD) with implicit solvent (IS) is used to elucidate the stability of LBs supported on silica substrates decorated with hydrophilic and hydrophobic NPs. We introduced novel features in IS-CGMD set-up, which (a) secure the iso-tension membrane condition and (b) account for long-range lipid-substrate interactions due to the existence of the nanometer thick hydration layers between LB and silica. The latter effect is incorporated by using the effective long-range potential of interactions between lipid heads and silica mimicking the disjoining pressure developed in the hydration layer. The proposed IS-GCMD method allowed for simulation of large systems with up to 40 nm NPs and 80,000 lipids in the simulation cell of $231 * 154 * 77\ nm^3$ in volume.

The main results of the simulations are as follows.

1. In studies of interactions of LB with a plane silica surface, we reproduced with our IS-CGMD model the results of earlier atomistic MD simulations showing the presence the hydration layer of water molecules confined between the substrate in two distinct configurations: α-states with the LB closely attached to the substrate and β-states with nm thick hydration layer. This effect is accounted by introducing the effective long-range lipid-silica potential that imitates the disjoining pressure in the hydration layer.

2. In simulations of the interaction of LB with hydrophilic NPs deposited on a silica substrate, we have found a dramatic dependence of the stability of SLB on the NP size, as demonstrated in the experiments of Roiter et al[28, 29]. We found that smaller NPs, from 1.54nm – 15 nm in diameter, induce holes in SLB and cannot be coated by the LB, while the membrane coating of NPs of size 23 and 40 nm was almost complete (within the limited length of our simulations). The coating defects at the bottom of NPs in highly curved regions can be attributed to (a) artificially acute geometry in the vicinity of the contact between a spherical particle and plane surface and (b) insufficient flexibility of the lipid model represented by the chain of three beads.

3. In simulations of the interaction of LB with hydrophobic NPs deposited on a silica substrate, we have found that smaller NP of a size smaller than bilayer thickness penetrates into the LB, yet are not fully encapsulated. As the NP size increases and the number of interactions between NP-LB increases due to the affinity between tails and the hydrophobic surface of NP, the lipid chains were able to reconfigure and to completely encapsulate the NP.

Although the obtained results look promising, further analyses and model modifications are needed to avoid the formation of membrane defects in highly curved regions. This can be done by refining (a) the coarse-grain lipid model allowing for the chain flexibility and (b) the implementation of the long-range lipid-surface potential, which was justified for the ideal plane geometry. The latter is a general problem of the implementation of the disjoining pressure effects for curved interfaces beyond the conventional Derjaguin approximation[38] which ignores the curvature effects.

In conclusions, with the implementation of the novel methods in IS-CGMD simulations, we simulated LB interactions with NP as large as 40 nm and got comparable results with the experimental observations on the stability of SLB on NP-decorated silica surfaces. The proposed method can be extended and applied to other NP-membrane systems, specifically to study the membrane stability affected by the presence of host bodies.

5. References:

1. Teli, M. K.; Mutalik, S.; Rajanikant, G. K., Nanotechnology and Nanomedicine: Going Small Means Aiming Big. *Current Pharmaceutical Design* **2010,** *16* (16), 1882-1892.
2. Kim, I.; Li, H. Q.; Shin, N. H.; Ha, C. S.; Suh, H.; Batt, C. A., Diacetylene Phospholipid-Mediated Synthesis of Germania Nanotubules and Nanoparticles. *Chemistry of Materials* **2009,** *21* (16), 3782-3787.
3. Ye, J. S.; Ottova, A.; Tien, H. T.; Sheu, F. S., Nanostructured platinum-lipid bilayer composite as biosensor. *Bioelectrochemistry* **2003,** *59* (1-2), 65-72.
4. Castellana, E. T.; Cremer, P. S., Solid supported lipid bilayers: From biophysical studies to sensor design. *Surface Science Reports* **2006,** *61* (10), 429-444.
5. Groves, J. T.; Dustin, M. L., Supported planar bilayers in studies on immune cell adhesion and communication. *Journal of Immunological Methods* **2003,** *278* (1-2), 19-32.
6. Knoll, W.; Naumann, R.; Friedrich, M.; Robertson, J. W. F.; Losche, M.; Heinrich, F.; McGillivray, D. J.; Schuster, B.; Gufler, P. C.; Pum, D.; Sleytr, U. B., Solid supported lipid membranes: New concepts for the biomimetic functionalization of solid surfaces. *Biointerphases* **2008,** *3* (2), FA125-FA135.
7. Richter, R. P.; Berat, R.; Brisson, A. R., Formation of solid-supported lipid bilayers: An integrated view. *Langmuir* **2006,** *22* (8), 3497-3505.
8. Sackmann, E., Supported membranes: Scientific and practical applications. *Science* **1996,** *271* (5245), 43-48.
9. Vishnyakov, A.; Li, T.; Neimark, A. V., Adhesion of Phospholipid Bilayers to Hydroxylated Silica: Existence of Nanometer-Thick Water Interlayers. *Langmuir* **2017,** *33* (45), 13148-13156.
10. Fischer, A.; Lösche, M.; Möhwald, H.; Sackmann, E., On the nature of the lipid monolayer phase transition. *Journal de Physique Lettres* **1984,** *45* (16), 785-791.
11. Eggl, P.; Pink, D.; Quinn, B.; Ringsdorf, H.; Sackmann, E., Diffusion in quasi two-dimensional macromolecular solutions. *Macromolecules* **1990,** *23* (14), 3472-3480.
12. Anderson, T. H., Formation of Supported Bilayers on Silica Substrates. . *Langmuir* **2009,** *25*, 6997-700.
13. Valtiner, M.; Donaldson, S. H.; Gebbie, M. A.; Israelachvili, J. N., Hydrophobic Forces, Electrostatic Steering, and Acid–Base Bridging between Atomically Smooth Self-Assembled Monolayers and End-Functionalized PEGolated Lipid Bilayers. *Journal of the American Chemical Society* **2012,** *134* (3), 1746-1753.
14. Rapp, M. V.; Donaldson, S. H.; Gebbie, M. A.; Gizaw, Y.; Koenig, P.; Roiter, Y.; Israelachvili, J. N., Effects of Surfactants and Polyelectrolytes on the Interaction between a Negatively Charged Surface and a Hydrophobic Polymer Surface. *Langmuir* **2015,** *31* (29), 8013-8021.
15. Yu, J.; Kan, Y.; Rapp, M.; Danner, E.; Wei, W.; Das, S.; Miller, D. R.; Chen, Y.; Waite, J. H.; Israelachvili, J. N., Adaptive hydrophobic and hydrophilic interactions of mussel foot proteins with organic thin films. *Proceedings of the National Academy of Sciences* **2013,** *110* (39), 15680-15685.
16. Donaldson, S. H.; Das, S.; Gebbie, M. A.; Rapp, M.; Jones, L. C.; Roiter, Y.; Koenig, P. H.; Gizaw, Y.; Israelachvili, J. N., Asymmetric Electrostatic and Hydrophobic–

Hydrophilic Interaction Forces between Mica Surfaces and Silicone Polymer Thin Films. *ACS Nano* **2013,** *7* (11), 10094-10104.
17. Das, C.; Sheikh, K. H.; Olmsted, P. D.; Connell, S. D., Nanoscale mechanical probing of supported lipid bilayers with atomic force microscopy. *Physical Review E* **2010,** *82* (4).
18. Schneider, J.; Barger, W.; Lee, G. U., Nanometer Scale Surface Properties of Supported Lipid Bilayers Measured with Hydrophobic and Hydrophilic Atomic Force Microscope Probes. *Langmuir* **2003,** *19* (5), 1899-1907.
19. Rico, F.; Abdulreda, M. H.; Moy, V. T.; Bhalla, A.; Chapman, E. R.; Berggren, P.-O., Pulling force generated by interacting SNAREs facilitates membrane hemifusion. *Integrative Biology* **2009,** *1* (4), 301-310.
20. Israelachvili, J. N.; Wennerstroem, H., Entropic forces between amphiphilic surfaces in liquids. *The Journal of Physical Chemistry* **1992,** *96* (2), 520-531.
21. Pera, I.; Stark, R.; Kappl, M.; Butt, H.-J.; Benfenati, F., Using the Atomic Force Microscope to Study the Interaction between Two Solid Supported Lipid Bilayers and the Influence of Synapsin I. *Biophysical Journal* **2004,** *87* (4), 2446-2455.
22. Kim, H. I.; Mate, C. M.; Hannibal, K. A.; Perry, S. S., How Disjoining Pressure Drives the Dewetting of a Polymer Film on a Silicon Surface. *Physical Review Letters* **1999,** *82* (17), 3496-3499.
23. Heine, D. R.; Rammohan, A. R.; Balakrishnan, J., Atomistic simulations of the interaction between lipid bilayers and substrates. *Molecular Simulation* **2007,** *33* (4-5), 391-397.
24. Roark, M.; Feller, S. E., Structure and Dynamics of a Fluid Phase Bilayer on a Solid Support as Observed by a Molecular Dynamics Computer Simulation. *Langmuir* **2008,** *24* (21), 12469-12473.
25. Pertsin, A.; Grunze, M., Possible mechanism of adhesion in a mica supported phospholipid bilayer. *Journal of Chemical Physics* **2014,** *140* (18), 8.
26. Xing, C. Y.; Faller, R., Interactions of lipid bilayers with supports: A coarse-grained molecular simulation study. *Journal of Physical Chemistry B* **2008,** *112* (23), 7086-7094.
27. Hoopes, M. I.; Deserno, M.; Longo, M. L.; Faller, R., Coarse-grained modeling of interactions of lipid bilayers with supports. *Journal of Chemical Physics* **2008,** *129* (17).
28. Roiter, Y.; Ornatska, M.; Rammohan, A. R.; Balakrishnan, J.; Heine, D. R.; Minko, S., Interaction of nanoparticles with lipid membrane. *Nano Letters* **2008,** *8* (3), 941-944.
29. Roiter, Y.; Ornatska, M.; Rammohan, A. R.; Balakrishnan, J.; Heine, D. R.; Minko, S., Interaction of Lipid Membrane with Nanostructured Surfaces. *Langmuir* **2009,** *25* (11), 6287-6299.
30. Lu, F.; Wu, S. H.; Hung, Y.; Mou, C. Y., Size Effect on Cell Uptake in Well-Suspended, Uniform Mesoporous Silica Nanoparticles. *Small* **2009,** *5* (12), 1408-1413.
31. Lin, Y. S.; Haynes, C. L., Impacts of Mesoporous Silica Nanoparticle Size, Pore Ordering, and Pore Integrity on Hemolytic Activity. *Journal of the American Chemical Society* **2010,** *132* (13), 4834-4842.
32. Burgess, S.; Vishnyakov, A.; Tsovko, C.; Neimark, A. V., Nanoparticle-Engendered Rupture of Lipid Membranes. *The Journal of Physical Chemistry Letters* **2018,** *9* (17), 4872-4877.

33. Noguchi, H.; Takasu, M., Self-assembly of amphiphiles into vesicles: A Brownian dynamics simulation. *Physical Review E* **2001,** *64* (4), 041913.
34. Drouffe, J.; Maggs, A.; Leibler, S., Computer simulations of self-assembled membranes. *Science* **1991,** *254* (5036), 1353-1356.
35. Brannigan, G.; Brown, F. L. H., Solvent-free simulations of fluid membrane bilayers. *Journal of Chemical Physics* **2004,** *120* (2), 1059-1071.
36. Farago, O., "Water-free" computer model for fluid bilayer membranes. *Journal of Chemical Physics* **2003,** *119* (1), 596-605.
37. Cooke, I. R.; Deserno, M., Solvent-free model for self-assembling fluid bilayer membranes: Stabilization of the fluid phase based on broad attractive tail potentials. *Journal of Chemical Physics* **2005,** *123* (22), 224710.
38. Israelachvili, J., Intermolecular and surface forces. Academic Press, London. *Intermolecular and surface forces. 2nd ed. Academic Press, London.* **1992**, -.
39. Tolpekina, T. V., et al. (2004). "Simulations of stable pores in membranes: System size dependence and line tension." The Journal of Chemical Physics **121**(16): 8014-8020.